

BEAM HEAT LOAD MEASUREMENTS WITH COLDDIAG AT THE DIAMOND LIGHT SOURCE

S. Gerstl*, S. Casalbuoni, A. W. Grau, D. Saez de Jauregui, T. Holubek, R. Voutta
 Karlsruhe Institute of Technology (KIT), Karlsruhe, Germany,
 R. Bartolini, M. P. Cox, E. C. Longhi, G. Rehm, J. C. Schouten,
 R. Walker, Diamond Light Source, Oxfordshire, England,
 M. Migliorati, B. Spataro, INFN/LNF, Frascati, Italy

Abstract

Understanding the heat load from an electron beam on a cold beam tube (liner) is an open issue of great interest for the cryogenic layout of superconducting insertion devices. COLDDIAG, a cold vacuum chamber for diagnostics was designed and built especially for this purpose. The instrumentation comprises temperature sensors, pressure gauges, mass spectrometers as well as retarding field analyzers with which it is possible to measure the beam heat load, total pressure, and gas content as well as the flux of particles hitting the chamber walls. COLDDIAG was installed in November 2011 in the Diamond Light Source (DLS). Due to a mechanical failure at one thermal transition, it was removed after only one week of operation. A redesign of the faulty transition in COLDDIAG allowed reinstallation in August 2012. In this work, we report on the measurements and results obtained during the first months since reinstallation in DLS.

INTRODUCTION

One of the open issues for the development of superconducting insertion devices is the understanding of the heat intake from the electron beam to the cold beam tube (liner). Possible beam heat load sources are synchrotron radiation, impedance due to geometric effects, resistive walls, and electron and/or ion bombardment. Although the values of the beam heat load on a cold bore have been measured at different light sources, the disagreement between measurements and calculations considering synchrotron radiation and resistive wall heating is not understood [1-3]. With the aim of measuring the beam heat load on a cold bore and the hope gaining a deeper understanding of the underlying mechanisms, a cold vacuum chamber for diagnostics was built [4]. The cryostat was first installed into the DLS storage ring in November 2011. Due to a mechanical failure of the thermal transition from the cold beam tube to the temperature shield the cryostat had to be removed after one week of operation. The results from this run are reported in Ref. [5]. Following a redesign of the broken transition and several other small changes, COLDDIAG was reassembled and successfully installed again in August 2012. In the following we briefly describe the experimental layout of COLDDIAG [4] and report results obtained during the first few months of operation at DLS

* stefan.gerstl@kit.edu, the stay abroad was supported by the Karlsruhe House of Young Scientists (KHYS)

after the second installation. The beam heat load, pressure, gas content and electron flux have been measured while varying the average beam current and for different filling patterns.

THE COLDDIAG EXPERIMENTAL SETUP

The cryostat is a cryogen free system, cooled with a Sumitomo RDK-415D cryocooler. A base temperature of around 6 K is reached on the liner in absence of beam, which is slightly higher than the base temperature reached

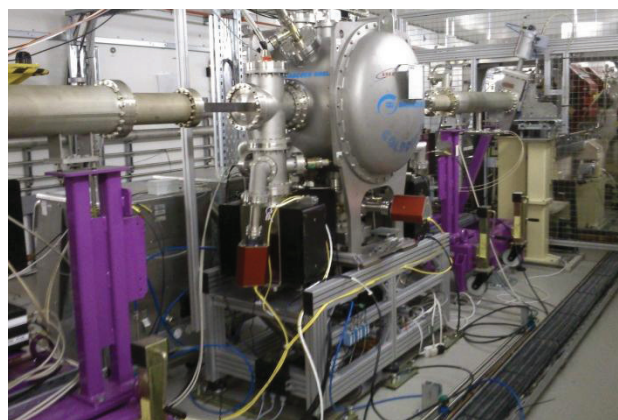


Figure 1: COLDDIAG installed at the DLS.

during the first installation which was 4 K. The cold section has a length of around 500 mm.

The electron beam passes through a 60 mm x 10 mm elliptical bore made from high purity copper block. Similar to the surface of the ANKA superconducting undulators, the inner surface of this beam tube is plated with 50 μm of copper.

In total 40 temperature sensors allow monitoring of the status of the chamber and the beam heat load. Six ceramic heaters are installed to simulate the heating from the beam (Fig. 1) and to calibrate the temperature to the corresponding heating power. A description of the calibration procedure can be found in Ref. [3].

In addition to the cold chamber, two 270 mm long warm sections are placed upstream and downstream. The three sections in COLDDIAG are each equipped with a residual gas analyser, a pressure gauge, and a retarding field analyser directly connected to the beam tube, to investigate the residual gas components and the electrons impinging the chamber wall. In order to suppress the low

energy electrons bombarding the wall, a solenoid on the beam axis producing a maximum field of 100 Gauss is wound around half of the cold section of the UHV chamber.

PRESSURE MEASUREMENTS

Figure 2 shows the pressure on the gauges located in the straight section upstream, downstream and in COLDDIAG as a function of the beam current. The measurement was performed with 3 GeV and 460 consecutive bunches separated by 2 ns. The pressure measured in the upstream pumping section has a linear dependence on the beam current, in contrast to the pressure measured with the other gauges. This linear behaviour is typical for photodesorption. To shade COLDDIAG from the direct synchrotron radiation created by the upstream bending magnet, a taper is installed between the upstream pumping station and the cryostat. The non-linear pressure increase after the taper demonstrates that the shading is sufficient and no

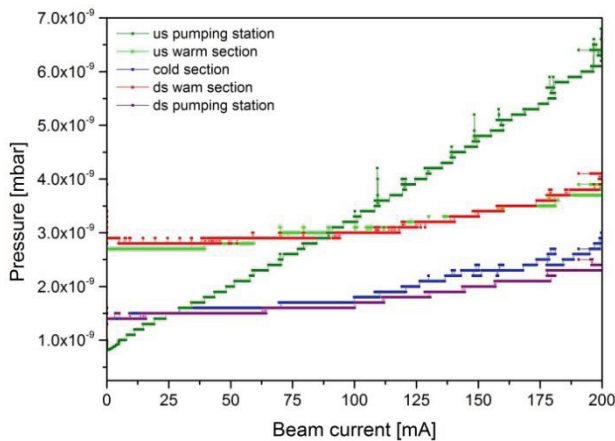


Figure 2: Pressure plotted against the average beam current for a filling pattern of 460 sequential bunches.

synchrotron radiation is hitting the liner of COLDDIAG. Synchrotron radiation can therefore be excluded as the dominant beam heat load source in COLDDIAG. However, reflected synchrotron radiation might fill the vacuum chamber without being the dominating mechanism of molecule desorption.

BEAM HEAT LOAD MEASUREMENTS

In Fig. 3 the beam heat load measured on the cold liner is plotted against the beam current for different filling patterns. The black curve shows the beam heat load for 900 bunches obtained with the old thermal transition in November 2011. During this current ramp the superconducting wigglers were not powered, which results in a smaller energy spread, thus reducing the bunch length by about 25%. As can be seen in the two 686 bunches measurements, with and without the wiggler magnets powered, a shorter bunch length causes higher beam heat load. Taking into account the different bunch

lengths a comparison of the 900 bunch filling pattern measured before and after the reinstallation (see red curve) shows good agreement.

Figure 3 also shows that the dependence of the heat

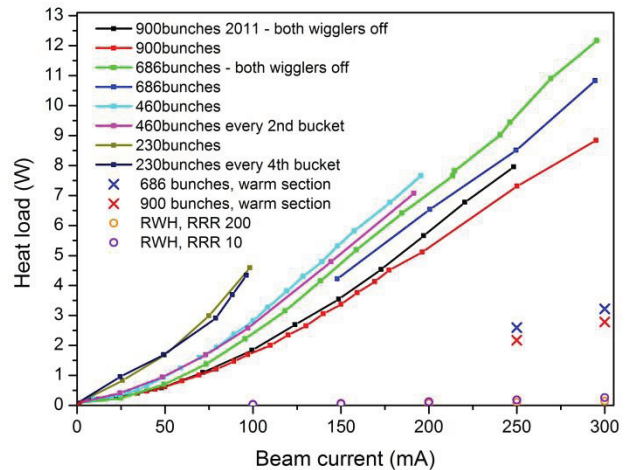


Figure 3: Beam heat load in COLDDIAG measured for different filling patterns as a function of the average beam current. The black curve was measured in 2011 during the first installation. The crosses are the beam heat load measured for the 270 mm long upstream warm sections. Predictions from resistive wall heating calculations for the cold liner section and RRR of 10 and 200 are indicated by circles.

load on the beam current is not linear. In addition to the pressure dependence shown before, this confirms that synchrotron radiation is not the main source of beam heat load.

Besides the non-linear relation between heat load and beam current, the dependence on the number of bunches can be seen in Fig. 3. The heat load increases with decreasing number of bunches, i.e. with increasing bunch current. The beam heat load due to geometrical and resistive wall impedance to COLDDIAG installed in DLS has been studied in Ref. [6]. The sum of the values of the beam heat load predicted from geometrical and resistive wall impedance is more than one order of magnitude below the measured values. In Fig. 3 the predicted values for resistive wall heating (RWH), taking into account the anomalous skin effect, for a residual resistance ratio (RRR) of 10 (violet circles) and 200 (orange circles), are shown.

Also shown in Fig. 3 are the values obtained for the upstream warm section (crosses) during user operation with 900 (red) and 686 (blue) bunches for an average beam current of 250 mA and 300 mA. Assuming resistive wall heating as the main heat load source, the measured values in the warm sections are expected to be higher compared with the values obtained for the cold section, since the resistance grows with increasing temperature. However, the data presented in Fig. 3 show the opposite behaviour.

ELECTRON ENERGY MEASUREMENTS

In each of the three liner sections a retarding field analyser (RFA) is installed to investigate the charged particles hitting the chamber walls. Measurements show that most of the particles hitting the wall have a negative charge [5]. Figure 4 shows the electron spectrum measured during user operation with a beam current of 300 mA, 686 bunches and top-up mode enabled. The negative retarding voltage is changed from 0 - 250 V in steps of 100 mV. For each retarding voltage the data are taken for one RFA after the other. The collector plate is biased with +50 V and the current is measured with a Keithley 6514 electrometer. The RFA setup works as a

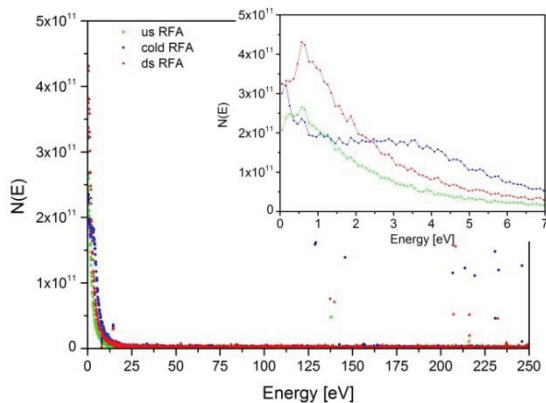


Figure 4: Energy spectrum from the three RFAs located upstream (us), downstream (ds) and in the cold section of COLDDIAG for 686 bunches and 300 mA beam current.

high pass filter, rejecting all electrons with energies below the retarding voltage. To obtain the spectrum shown in Fig. 4, the derivative of the current measured for two consecutive energies has to be calculated. The measurements show that most electrons hitting the RFAs have energies below 10 eV. For the room temperature data, similar behaviour has been observed at ANKA [7]: a zoom into the energy range from 0 - 7 eV shows in the upstream and downstream warm section a peak of the spectrum slightly below 1 eV, whereas, the RFA spectrum in the cold section shows a peak around 0 eV and a second broader peak around 3.5 eV. A rough estimation of the heating power created by electron bombardment can be obtained by assuming that all electrons hitting the cold RFA have a peak energy of 3.5 eV. Using a relatively simple model the heating power P is given by $P = \Delta W \dot{N}$, where \dot{N} is the number of electrons per second hitting the cold liner and ΔW is the transferred energy [2]. Considering the above parameters, the resulting heat load is less than 1 mW. However, the measured energy spectrum and flux might only show a fraction of the actual number of electrons hitting the wall, because the location of the RFAs could be unfortunate and the maximum detectable energy is limited to 250 eV. Moreover, the small acceptance angle of the RFA for particles with high energies traveling with a velocity component in beam direction can also reduce the amount of detected electrons.

TEMPERATURE DISTRIBUTION ON THE COLD LINER

Figure 5 shows the temperature distribution for the sensors placed along the liner during a user run for 686 bunches and 300 mA after reaching thermal equilibrium. While the temperatures during the calibration, for the same heating power, are within ± 0.2 K, the values with

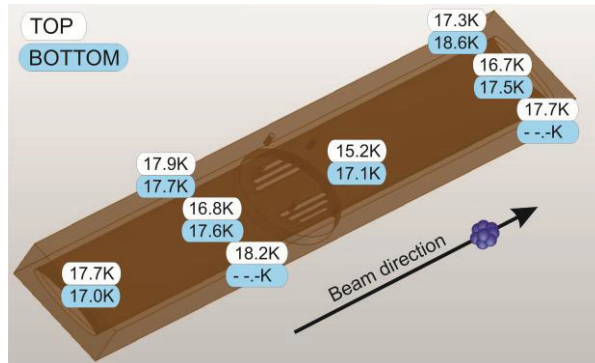


Figure 5: Temperature distribution on the cold liner section during user run with 686 bunches for a beam current of 300 mA and top-up operation.

beam range from 15.2 K to 18.6 K. As the liner is made from a single high purity copper block even small temperature gradients must be caused by large differences in the heating power. This indicates a highly non-uniform beam heat load distribution which cannot be explained by resistive wall impedance effects.

CONCLUSION

COLDDIAG was reinstalled in the storage ring at the Diamond Light Source in August 2012 after a redesign of the previously failed thermal transition. Since then, the beam heat load has been measured for different filling patterns and beam currents. The data obtained are in good agreement with the values measured during the short first installation. In addition measurements of the electron energy spectrum, the total pressure and gas content have been performed. Experimental and theoretical work is ongoing, with the aim of explaining the very high measured beam heat load compared with existing theories.

REFERENCES

- [1] E. Wallèn, G. LeBlanc, Cryogenics 44, 879 (2004).
- [2] S. Casalbuoni et al., Phys. Rev. ST Accel. Beams 10, 093202 (2007).
- [3] S. Casalbuoni et al., Proceedings of EPAC08.
- [4] S. Gerstl et al., Proceedings of IPAC10; S. Casalbuoni et al., IEEE Trans. on Appl. Supercond. 1760-1763 Vol. 21-3 (2011).
- [5] S. Gerstl et al., Proceedings of IPAC12.
- [6] S. Casalbuoni, et al., 2012 JINST 7 P11008.
- [7] D. Saez de Jauregui et al., Proceedings of PAC 2009.